

Crescent states in charge-imbalanced polariton condensates

Artem Strashko,¹ Francesca M. Marchetti,² Allan H. MacDonald,³ and Jonathan Keeling⁴

¹Center for Computational Quantum Physics, Flatiron Institute, 162 5th Avenue, New York, NY 10010, USA

²Departamento de Física Teórica de la Materia Condensada & Condensed Matter Physics Center (IFIMAC), Universidad Autónoma de Madrid, Madrid 28049, Spain

³Department of Physics, University of Texas, Austin, Texas 78712, USA

⁴SUPA, School of Physics and Astronomy, University of St Andrews, St Andrews, KY16 9SS, United Kingdom

(Dated: February 6, 2022)

We study two-dimensional charge-imbalanced electron-hole systems embedded in an optical microcavity. We find that strong coupling to photons favors states with pairing at zero or small center of mass momentum, leading to a condensed state with spontaneously broken time-reversal and rotational symmetry, and unpaired carriers that occupy an anisotropic crescent-shaped sliver of momentum space. The crescent state is favoured at moderate charge imbalance, while a Fulde-Ferrel-Larkin-Ovchinnikov-like state — with pairing at large center of mass momentum — occurs instead at strong imbalance. The crescent state stability results from long-range Coulomb interactions in combination with extremely long-range photon-mediated interactions.

Introduction— At low-carrier densities, electrons and holes in two-dimensional semiconductors pair into bosonic excitons that can condense at low enough temperatures [1–5]. Exciton condensation is expected to survive the frustration of unequal electron and hole densities [6–10], which favors condensed electron-hole pairs that acquire a finite centre-of-mass momentum forming a state similar to the Fulde-Ferrel [11] (FF) and Larkin-Ovchinnikov [12] (LO) phases (abbreviated as FFLO) known from superconductors. The prospect of FFLO phases has also been extensively discussed in the context of cold atoms [13]. Although FFLO phases are common to imbalanced two-component fermions with attractive interactions, more exotic alternatives, such as phase separation in momentum space (also named “breached pair” or “Sarma” phases) have been suggested in special cases [14, 15]. In neutral systems, these uniform density imbalanced phases compete with, and are largely replaced by, phase separation in real space [16–18]. For the charged electron-hole systems we focus on here, however, the electrostatic energy forbids phase separation and exotic uniform states are a stronger possibility.

The boson condensation temperature increases significantly when optically-pumped two-dimensional semiconductors are placed in a planar microcavity, designed so that long-wavelength confined photons are close to resonance with excitons [19, 20]. The resulting quasiparticles, exciton-polaritons, are photon-exciton hybrids, that have a greatly reduced mass [21]. This favors long-range coherence, and yields condensates that are more robust than without a cavity [22]. In this Letter we examine the influence of a resonant planar microcavity on condensation phenomena in 2D semiconductor structures with unequal electron and hole densities — see Fig. 1(a-b). We find strong matter-light coupling favors small pairing-momentum states over FFLO states with larger pairing momentum — specifically it induces breached pair states and anisotropic crescent states, explained below, which

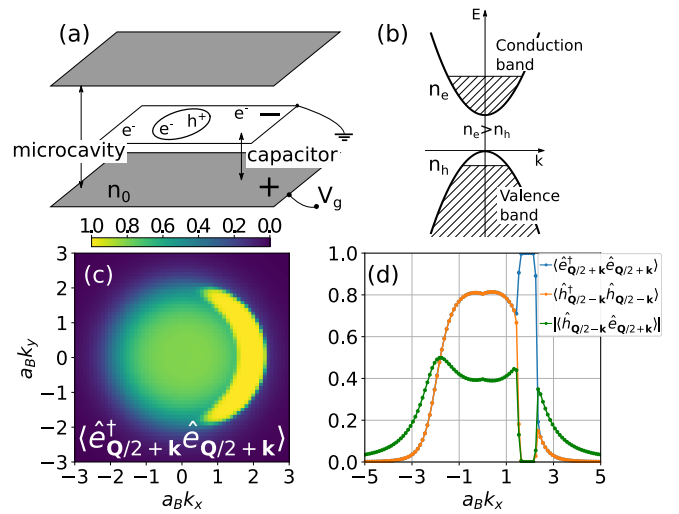


Figure 1. (a) Semiconductor quantum well embedded in a planar microcavity, with net charge tuned by a gate voltage between the bottom mirror and the grounded semiconductor. (b) Occupied bands with finite excitation and charge. (c) Typical anisotropic crescent state, represented by the electron occupation numbers, which reaches one at low temperatures inside the yellow crescent-shaped region. (d) $k_y = 0$ momentum space slice of (c), showing both occupations and electron-hole coherence. Inside the Fermi surface (yellow in (c)), both conduction and valence bands are occupied so coherence vanishes. Elsewhere in momentum space only one state is occupied. Results were calculated using the model parameters explained in the text: target charge density $n_0 = 8.125 \times 10^{-2} a_B^{-2}$, excitation chemical potential relative to band gap $\mu_{ex} - E_G = E_B$, temperature $k_B T = 0.04 E_B$, photon cutoff frequency $\omega_0 = 3.06 E_B$, matter-light coupling momentum cutoff $\kappa = 2.5 a_B^{-1}$, matter-light coupling $g_0 = 0.8 E_B a_B$, mass ratio $m_e/m_h = 1$, $\varepsilon = 1$, and capacitive energy $\alpha = 800 E_B a_B^2$.

spontaneously break both rotational and time-reversal symmetry. The anisotropic states place excess carriers in a compact crescent-shaped sliver in momentum

space on the edge of the region occupied by electron-hole pairs, as illustrated in Figs. 1(c-d), instead of spreading them isotropically. The crescent and breached pair states arise only because of coupling to light, and are stabilized by the small photon mass. Further, as discussed later, the anisotropy also requires long-range Coulomb interactions. As such, while the electron-hole-photon model we will introduce below is superficially similar to the two-channel model of ultracold fermionic atoms [23], there are crucial differences: For atoms, interactions are contact-like and, most importantly, the analogue of the photon is a “closed channel” molecular state, with a mass twice that of the atoms. In addition, phase separation in real space dominates the phase diagram of cold atoms [16–18]. The states we propose here are therefore unique to polaritonic systems. The new crescent states can be identified experimentally by strongly anisotropic electrical transport characteristics that can be reoriented by altering the polariton-confinement landscapes or by weak resonant optical excitation. In the following we first explain the calculations that allow us to predict the crescent states, and then discuss properties that could identify them experimentally.

Model— We consider a model of electrons and holes confined in two-dimensional (2D) quantum wells, subject to Coulomb interactions, and coupled to cavity photons. The Hamiltonian is thus ($\hbar = 1$, $4\pi\epsilon_0 = 1$):

$$\begin{aligned} \hat{H} = & \sum_{\mathbf{k}} \left[\left(\frac{k^2}{2m_e} + E_G \right) \hat{e}_{\mathbf{k}}^\dagger \hat{e}_{\mathbf{k}} + \frac{k^2}{2m_h} \hat{h}_{\mathbf{k}}^\dagger \hat{h}_{\mathbf{k}} \right] \\ & + \frac{1}{2S} \sum_{\mathbf{k}, \mathbf{k}', \mathbf{p}} V_{\mathbf{p}} \left\{ \hat{e}_{\mathbf{k}+\mathbf{p}}^\dagger \hat{e}_{\mathbf{k}'-\mathbf{p}}^\dagger \hat{e}_{\mathbf{k}'} \hat{e}_{\mathbf{k}} + \hat{h}_{\mathbf{k}+\mathbf{p}}^\dagger \hat{h}_{\mathbf{k}'-\mathbf{p}}^\dagger \hat{h}_{\mathbf{k}'} \hat{h}_{\mathbf{k}} \right. \\ & \left. - 2\hat{e}_{\mathbf{k}+\mathbf{p}}^\dagger \hat{h}_{\mathbf{k}'-\mathbf{p}}^\dagger \hat{h}_{\mathbf{k}'} \hat{e}_{\mathbf{k}} \right\} + \alpha S (\hat{n}_c - n_0)^2 \\ & + \sum_{\mathbf{k}} \omega_{\mathbf{k}} \hat{a}_{\mathbf{k}}^\dagger \hat{a}_{\mathbf{k}} + \sum_{\mathbf{k}, \mathbf{p}} \frac{g_{\mathbf{k}}}{\sqrt{S}} \left(\hat{e}_{\mathbf{k}}^\dagger \hat{h}_{\mathbf{p}-\mathbf{k}}^\dagger \hat{a}_{\mathbf{p}} + \hat{a}_{\mathbf{p}}^\dagger \hat{h}_{\mathbf{p}-\mathbf{k}} \hat{e}_{\mathbf{k}} \right), \quad (1) \end{aligned}$$

where S is the system area. The first term in \hat{H} describes non-interacting electrons and holes with masses m_e and m_h in a two-dimensional semiconductor with band gap E_G . The second term is the mutual Coulomb interaction $V_{\mathbf{p}} = 2\pi e^2/\epsilon p$, while the third term gives the dependence of the electrostatic energy on the system charge density. Here $\alpha = e^2 S/2C$ is an (intensive) capacitive scale, which depends on the gating geometry. The target charge density, n_0 , is proportional to a tunable gate voltage. Typically α is large compared to the corresponding interaction scale ($e^2 n_e^{-1/2}/\epsilon$) so that the actual charge imbalance which minimizes the free energy is nearly identical to the target charge density, i.e. $\langle \hat{n}_c \rangle \simeq n_0$, where

$$\hat{n}_c = \frac{1}{S} \sum_{\mathbf{k}} \left(\hat{e}_{\mathbf{k}}^\dagger \hat{e}_{\mathbf{k}} - \hat{h}_{\mathbf{k}}^\dagger \hat{h}_{\mathbf{k}} \right) = \hat{n}_e - \hat{n}_h. \quad (2)$$

Including the electrostatic energy realistically, as we do in Eq. (1), allows us to use the grand-canonical ensemble

without generating unphysical phase separations, and thereby allows us to consider more general variational ansatz states. The final line of Eq. (1) accounts for the cavity photons and their coupling to electrons and holes. We assume a single branch of cavity photons, and approximate the dispersion as quadratic, $\omega_{\mathbf{k}} = \omega_0 + k^2/2m_{ph}$, with typical mass $m_{ph} \simeq 10^{-4}m_e$. In the following we measure lengths in units of the 2D exciton Bohr radius $a_B = \epsilon/(2\mu e^2)$, where $\mu = m_e m_h/(m_e + m_h)$, and energies in units of $E_B = 1/(2\mu a_B^2)$.

To avoid the ultraviolet divergences produced by a momentum-independent matter-light coupling [24–28], we take $g_{\mathbf{k}} = g_0 e^{-|\mathbf{k}|/\kappa}$, and choose $1/\kappa$ to be of the order of the material lattice constant. This cutoff breaks the theory gauge invariance under the replacement $\hat{e}_{\mathbf{k}} \rightarrow \hat{e}_{\mathbf{k}+e\mathbf{A}}$, $\hat{h}_{\mathbf{k}} \rightarrow \hat{h}_{\mathbf{k}-e\mathbf{A}}$, which could be recovered by taking $\kappa \rightarrow \infty$ and renormalizing the photon frequency; see Refs. [28, 29]. Full gauge invariance requires consistency of the band and matter-light coupling Hamiltonians [30], and is crucial to recover the no-go theorems precluding ground state superradiance [30, 31].

To control the excitation density we introduce a chemical potential μ_{ex} , and replace $\hat{H} \rightarrow \hat{H} - S\mu_{ex}\hat{n}_{ex}$, where

$$\hat{n}_{ex} = \frac{1}{S} \sum_{\mathbf{k}} \left[\hat{a}_{\mathbf{k}}^\dagger \hat{a}_{\mathbf{k}} + \frac{1}{2} \left(\hat{e}_{\mathbf{k}}^\dagger \hat{e}_{\mathbf{k}} + \hat{h}_{\mathbf{k}}^\dagger \hat{h}_{\mathbf{k}} \right) \right]. \quad (3)$$

The energy shift accounts for the time-dependence of the non-equilibrium condensates that form at finite excitation density. The no-go theorem does not apply for a system at finite excitation density [32]. We note that because we make the rotating wave approximation, equal shifts in ω_0 , E_G and μ_{ex} have no effect.

Variational approach— To estimate the *finite temperature* phase diagram of our model, we use a variational ansatz for the density matrix [33], $\hat{\rho}_v = \exp(-\beta \hat{H}_v)/\mathcal{Z}_v$, $\mathcal{Z}_v = \text{Tr}[\exp(-\beta \hat{H}_v)]$. We then minimise the free energy corresponding to this density matrix, $F_v = \langle \hat{H} \rangle_v + k_B T \text{Tr}[\hat{\rho}_v \ln \hat{\rho}_v] = \langle \hat{H} - \hat{H}_v \rangle_v - k_B T \ln \mathcal{Z}_v$, where $\langle \hat{X} \rangle_v = \text{Tr}(\hat{\rho}_v \hat{X})$. Standard thermodynamic identities allow one to show that F_v is an upper bound on the true free energy. The variational Hamiltonian \hat{H}_v should be chosen to be solvable, and for our model, we should allow for electron-hole coherence, photon coherence, population imbalance, and arbitrary polariton momentum \mathbf{Q} . We therefore consider a variational Hamiltonian of the form:

$$\begin{aligned} \hat{H}_v = & \nu_{\mathbf{Q}} \sqrt{S} \phi (\hat{a}_{\mathbf{Q}}^\dagger + \hat{a}_{\mathbf{Q}}) + \sum_{\mathbf{q}} \nu_{\mathbf{q}} \hat{a}_{\mathbf{q}}^\dagger \hat{a}_{\mathbf{q}} \\ & + \sum_{\mathbf{k}} \left(\hat{e}_{\frac{\mathbf{Q}}{2}+\mathbf{k}}^\dagger \hat{h}_{\frac{\mathbf{Q}}{2}-\mathbf{k}} \right) \begin{pmatrix} \eta_{\mathbf{k}}^e & \Delta_{\mathbf{k}} \\ \Delta_{\mathbf{k}} & -\eta_{\mathbf{k}}^h \end{pmatrix} \begin{pmatrix} \hat{e}_{\frac{\mathbf{Q}}{2}+\mathbf{k}} \\ \hat{h}_{\frac{\mathbf{Q}}{2}-\mathbf{k}}^\dagger \end{pmatrix}. \quad (4) \end{aligned}$$

We can derive an expression for F_v in terms of the eigenvalues and eigenstates of \hat{H}_v (see supplemental material [29]). The first term in Eq. (4) is chosen so that

the photon density is ϕ^2 . The results below are then obtained by minimizing over the variational parameters $(\phi, \nu_{\mathbf{q}}, \eta_{\mathbf{k}}^e, \eta_{\mathbf{k}}^h, \Delta_{\mathbf{k}}, \mathbf{Q})$. Because this ansatz contains only pairing of fermions and displacement of bosons, it is equivalent to mean field theory approaches.

Pairing phases— Previous work [10] explored the ground-state phase diagram of Eq.(1) in the absence of coupling to photons, using the grand canonical ensemble with a charge imbalance chemical potential μ_c ($\hat{H} \rightarrow \hat{H} - \mu_c S \hat{n}_c$) in place of a realistic electrostatic energy [34]. It predicted first order phase transitions between a balanced condensate with $\langle \hat{n}_c \rangle = 0$ and an imbalanced $\langle \hat{n}_c \rangle \neq 0$ anisotropic FFLO condensate with non-zero center-of-mass momentum $Q \sim |\langle \hat{n}_e \rangle^{1/2} - \langle \hat{n}_h \rangle^{1/2}|$. When applied to the exciton only problem, our more realistic description of electrostatics shows that the transition between a $\mathbf{Q} = \mathbf{0}$ condensate and the FFLO state (see Ref. [29]) is continuous as a function of gate voltage.

When the balanced condensate is coupled to photons, it becomes a polaritonic state, with exciton–photon coherence, further lowering its energy. In contrast, coupling to photons has little influence on the FF state because excitons with center of mass momentum \mathbf{Q} couple to photons at the same momentum, and the small photon mass places these far off resonance. The photon fraction in the FF state is therefore very small, and we thus refer to this state as dark. Coupling to photons therefore favors states with a small center of mass momentum. Numerical minimization indeed reveals that, at moderate imbalance, coupling to photons yields a bright polaritonic condensate state with \mathbf{Q} small but non-zero. Surprisingly, this state accommodates excess charged carriers by spontaneously breaking rotational and time reversal symmetry. At larger imbalance, the expected FF phase is recovered — for the extremely charge imbalanced case, see Ref. [35].

Figure 2 shows how the electron momentum distribution changes with charge imbalance — corresponding cross sections showing also hole occupation and coherence are presented in [29]. Panel (a) shows the case with $n_0 = 0$, i.e. balanced populations. At small n_0 (panel (b)), the state maintains $\mathbf{Q} = \mathbf{0}$ to take optimal advantage of the photon-mediated electron-hole coupling. In the zero temperature limit, accommodating extra charges requires forming a Fermi surface, which encloses regions of momentum space in which both valence and conduction band states are occupied. At low charge imbalance, the Fermi sea forms a ring at the outer edge of the region of paired electrons. We will refer to the state at low carrier densities as a “weak breached pair” (WBP) state, as it is reminiscent of the two-Fermi surface breached pair state described in Ref. [15]. In contrast to the fully breached pair, the coherence in Fig. 2(b), is only weakly suppressed in the region where extra electrons exist because the temperature is comparable to the conduction band Fermi energy. For intermediate

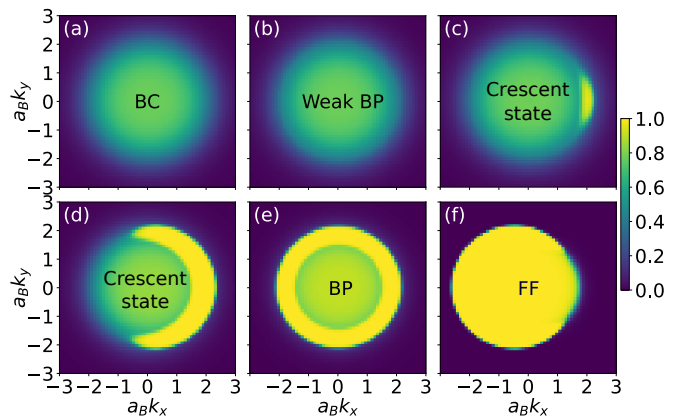


Figure 2. Electron occupation $\langle \hat{e}_{\mathbf{Q}/2+\mathbf{k}}^\dagger \hat{e}_{\mathbf{Q}/2+\mathbf{k}} \rangle$ for various imbalance values $n_0 a_B^2$: (a) 0, (b) 6.25×10^{-3} , (c) 1.875×10^{-2} , (d) 0.125, (e) 0.1875, (f) 0.25. Labels on each panel indicate the phases as described in the text. The values of $Q a_B$ are (c) 0.5×10^{-6} , (d) 0.5×10^{-5} , (f) 1.05, and zero for panels (a),(b),(e). Other parameters are as in Fig. 1.

values of n_0 , illustrated in panels (c,d), we find a surprising broken rotational symmetry anisotropic state with $0 < Q \ll |\langle \hat{n}_e \rangle^{1/2} - \langle \hat{n}_h \rangle^{1/2}|$. The unpaired carriers in this state are contained in a Fermi pocket with a crescent shape on the edge of the otherwise circular electron distribution, hence we refer to it as the crescent state (CS). As n_0 increases further, the crescent extends in angle. Eventually it is replaced by a filled annulus (panel e), equivalent to the breached pair (BP) state of Ref. [15], and related to the Sarma state [14]. Finally, at large enough n_0 , one recovers the dark FF state. Further increasing n_0 brings the system to a normal state (not shown). This sequence occurs at high excitation density. At low excitation density (not shown) the BP state is replaced by a Sarma state where excess particles occupy a single isotropic Fermi surface [14], matching the extreme imbalance limit [35].

Phase diagram — Figure 3 illustrates how the minimum free energy state evolves with target charge density and temperature by plotting charge imbalance, electronic excitation density, photon density, and anisotropy $\mathcal{A} \equiv \sum_{\mathbf{k}} |\hat{\mathbf{k}} \cdot \hat{\mathbf{Q}}| \langle \hat{e}_{\mathbf{Q}/2+\mathbf{k}}^\dagger \hat{e}_{\mathbf{Q}/2+\mathbf{k}} \rangle / \sum_{\mathbf{k}} \langle \hat{e}_{\mathbf{Q}/2+\mathbf{k}}^\dagger \hat{e}_{\mathbf{Q}/2+\mathbf{k}} \rangle$. This figure demonstrates that that the crescent state persists over a wide temperature range, before being replaced by the weakly breached pair (isotropic) state. From this figure we see that most transitions, other than those into and out of the BP state are continuous.

The quantities plotted in Fig. 3 allow us to classify the phases, and extract the phase diagrams in Fig. 4. Because the BP and crescent states have significant photon fractions, the small photon mass should allow them to survive to high temperature even when the collective fluctuations (absent in our mean-field theory) are included [36]. In contrast, the excitonic FF state should

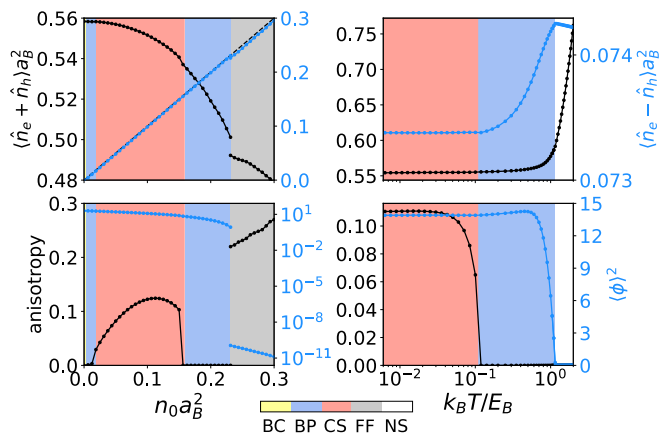


Figure 3. Evolution of state with target charge density n_0 at $k_B T = 0.04 E_B$ (left) and with temperature T at $n_0 a_B^2 = 0.075$ (right); other parameters as in Fig. 1. Top panels show excitonic density (black; left axis) and charge imbalance (blue; right axis). The dashed blue line shows n_0 . Bottom panels show anisotropy (black; left axis) and photon density ϕ^2 (blue; right axis).

be restricted to low temperatures, due to the larger excitonic mass. Since the crescent state is stabilised by the matter-light coupling, an experimentally accessible way to alter its robustness is by changing the photon cutoff frequency, ω_0 , *e.g.*, using a wedge cavity. When the photon is detuned far above the exciton energy, the cavity plays little role and excitonic results should be recovered. Figure 4(a) shows such a phase diagram, *vs.* n_0 and ω_0 . Because physical states require $\mu_{ex} < \omega_0$, the lower boundary of this phase diagram cuts off just above this limit. As expected the crescent state becomes less prominent with increasing ω_0 , although a narrow stability interval persists up to large detunings.

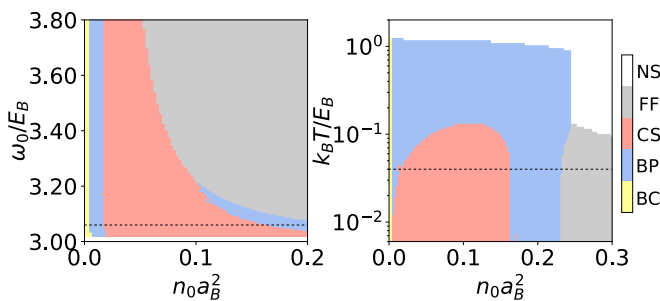


Figure 4. Phase diagrams. Left: *vs.* charge density n_0 and photon cutoff frequency ω_0 at $k_B T = 0.04 E_B$. Right: *vs.* charge density n_0 and temperature T at $\omega_0 = 3.06 E_B$. The dashed lines indicate $\omega_0 = 3.06 E_B$ (left) and $k_B T = 0.04 E_B$ respectively. All other parameters are as in Fig. 1.

Crescent State Properties— The crescent state is anisotropic, like the FF state, but has a significant photon fraction and a qualitatively smaller pairing momentum. Because of its anisotropy, it is not immediately clear

whether it has zero net current as expected by Bloch’s theorem [37]. An explicit calculation shows that the crescent state has a non-zero excitonic current (electron current plus hole current) that is balanced by an equal and opposite photon current — *i.e.* a counterflow condensate state — generated by a shift in the condensate pair momentum from $\mathbf{Q} = \mathbf{0}$ to $\mathbf{Q}_{min} \neq 0$ [38]. The momentum shift balances matter energy gain against photon kinetic energy cost. Since the shift is small enough to leave the electron and hole distributions almost unchanged, we can approximate $\mathbf{Q}_{min} \simeq (m_{ph}/|\phi|^2)[\sum_{\mathbf{k}} \mathbf{k}(\langle \hat{e}_{\mathbf{k}}^\dagger \hat{e}_{\mathbf{k}} \rangle/m_e + \langle \hat{h}_{\mathbf{k}}^\dagger \hat{h}_{\mathbf{k}} \rangle/m_h)]$, *i.e.*, $|\mathbf{Q}_{min}|$ is parametrically small due to the small photon to electron mass ratio. Indeed, as noted in the caption of Fig. 2, our numerical results for $|\mathbf{Q}_{min}|$ in the crescent state are orders of magnitude smaller than in the FF state.

Since Bloch’s theorem [37] can be generalized to a coupled photon-matter system, we expect that the charge current (electron current minus hole current) also vanishes. In our numerical calculations, we find that this cancellation is imperfect, but ascribe the non-zero numerical result to the UV matter-light coupling cutoff κ discussed previously. In the supplemental material [29], we show that this charge current vanishes as the UV cutoff diverges.

The crescent state is a metal with a Fermi surface for unpaired electrons, and we expect that it will exhibit metallic transport properties. The anisotropic Fermi surface in Fig. 2 implies anisotropic electrical transport with larger conduction along the thin direction of the crescent, *i.e.* in the direction parallel to \mathbf{Q} , that can be used to identify the crescent state experimentally. Any weak perturbation, for example weak resonant excitation or spatial anisotropy of a weak polariton confinement landscape, can be used to control the sense of anisotropy — possibly *in situ*. Also, since the crescent state breaks inversion symmetry, nonlinear *ac* response is also expected to exhibit rectification.

Notably, both strong matter-light coupling and long-range Coulomb interactions are required to stabilize the CS crescent state. While the photon promotes $\mathbf{Q} \approx \mathbf{0}$ pairing, it is the long-range Coulomb interaction which favors anisotropy. Indeed, screening the Coulomb interaction eventually leads to a continuous transition from the anisotropic crescent state to an isotropic state (see Ref. [29]). We therefore expect that our mean-field calculations overestimate the stability range of the crescent state.

Conclusions— Since the crescent and breached pair unbalanced states are polaritonic, they are expected to survive to high temperatures and should therefore be accessible in current experiments involving doped quantum wells [39–44] or two-dimensional materials in cavities [45–47]. Our work focuses on the small imbalance regime where we are most confident about our conclusions. At

high doping, one instead may consider Fermi-edge (Mahan) excitons, see e.g. [48, 49] and refs. therein. Open questions include how the states we consider here connect to these Fermi-edge states, the effects of electronic screening in a charge doped system, and practical treatments that go beyond mean-field theory.

Acknowledgments— We acknowledge helpful discussions with J. Levinsen, M. Parish, and P. Pieri. The Flatiron Institute is a division of the Simons Foundation. AS acknowledges support from the EPSRC CM-CDT (EP/L015110/1) and a travel award from the Scottish Universities Physics Alliance. AS, AHM and JK acknowledge financial support from a Royal Society International Exchange Award, IES\R2\170213. FMM acknowledges financial support from the Ministerio de Economía y Competitividad (MINECO), project No. MAT2017-83772-R. JK acknowledges financial support from EPSRC program “Hybrid Polaritonics” (EP/M025330/1). AHM acknowledges support from Army Research Office (ARO) Grant # W911NF-17-1-0312 (MURI). This work was performed in part at Aspen Center for Physics, which is supported by National Science Foundation grant PHY-1607611 and partially supported by a grant from the Simons Foundation.

-
- [1] L. Keldysh and Y. V. Kopayev, *Possible instability of the semimetal state with respect to Coulomb interaction*, Soviet Physics, Solid state **6**, 2219 (1964).
- [2] C. Comte and P. Nozières, *Exciton Bose Condensation: the ground state of an electron-hole gas I. Mean field description of a simplified model*, J. Phys. **43**, 1069 (1982).
- [3] A. A. High, J. R. Leonard, A. T. Hammack, M. M. Fogler, L. V. Butov, A. V. Kavokin, K. L. Campman, and A. C. Gossard, *Spontaneous coherence in a cold exciton gas*, Nature **483**, 584 (2012).
- [4] M. Fogler, L. Butov, and K. Novoselov, *High-temperature superfluidity with indirect excitons in van der Waals heterostructures*, Nat. Commun. **5**, 4555 (2014).
- [5] Z. Wang, D. A. Rhodes, K. Watanabe, T. Taniguchi, J. C. Hone, J. Shan, and K. F. Mak, *Evidence of high-temperature exciton condensation in two-dimensional atomic double layers*, Nature **574**, 76 (2019).
- [6] P. Pieri, D. Neilson, and G. C. Strinati, *Effects of density imbalance on the BCS-BEC crossover in semiconductor electron-hole bilayers*, Phys. Rev. B **75**, 113301 (2007).
- [7] A. L. Subasi, P. Pieri, G. Senatore, and B. Tanatar, *Stability of Sarma phases in density imbalanced electron-hole bilayer systems*, Phys. Rev. B **81**, 075436 (2010).
- [8] Y. Kazuo, A. Kenichi, and O. Takuma, *Quantum Condensation in ElectronHole Bilayers with Density Imbalance*, J. Phys. Soc. Japan **79**, 33001 (2010).
- [9] M. M. Parish, F. M. Marchetti, and P. B. Littlewood, *Supersolidity in electron-hole bilayers with a large density imbalance*, EPL (Europhysics Letters) **95**, 27007 (2011).
- [10] J. R. Varley and D. K. K. Lee, *Structure of exciton condensates in imbalanced electron-hole bilayers*, Phys. Rev. B **94**, 174519 (2016).
- [11] P. Fulde and R. A. Ferrell, *Superconductivity in a Strong Spin-Exchange Field*, Phys. Rev. **135**, A550 (1964).
- [12] A. I. Larkin and Y. N. Ovchinnikov, *Nonuniform state of superconductors*, Zh. Eksp. Teor. Fiz. **47**, 1136 (1964), [Sov. Phys. JETP **20**, 762(1965)].
- [13] D. E. Sheehy and L. Radzihovsky, *BEC-BCS crossover, phase transitions and phase separation in polarized resonantly-paired superfluids*, Ann. Phys. (N. Y). **322**, 1790 (2007).
- [14] G. Sarma, *On the influence of a uniform exchange field acting on the spins of the conduction electrons in a superconductor*, J. Phys. Chem. Solids **24**, 1029 (1963).
- [15] M. M. Forbes, E. Gubankova, W. V. Liu, and F. Wilczek, *Stability Criteria for Breached-Pair Superfluidity*, Phys. Rev. Lett. **94**, 017001 (2005).
- [16] M. W. Zwierlein, A. Schirotzek, C. H. Schunck, and W. Ketterle, *Fermionic superfluidity with imbalanced spin populations*, Science **311**, 492 (2006).
- [17] G. B. Partridge, W. Li, R. I. Kamar, Y.-a. Liao, and R. G. Hulet, *Pairing and phase separation in a polarized Fermi gas*, Science **311**, 503 (2006).
- [18] Y. Shin, M. W. Zwierlein, C. H. Schunck, A. Schirotzek, and W. Ketterle, *Observation of Phase Separation in a Strongly Interacting Imbalanced Fermi Gas*, Phys. Rev. Lett. **97**, 030401 (2006).
- [19] J. Kasprzak, M. Richard, S. Kundermann, A. Baas, P. Jeambrun, J. M. J. Keeling, F. M. Marchetti, M. H. Szymańska, R. André, J. L. Staehli, V. Savona, P. B. Littlewood, B. Deveaud, and L. S. Dang, *Bose-Einstein condensation of exciton polaritons.*, Nature **443**, 409 (2006).
- [20] R. Balili, V. Hartwell, D. Snoko, L. Pfeiffer, and K. West, *Bose-Einstein condensation of microcavity polaritons in a trap.*, Science **316**, 1007 (2007).
- [21] C. Weisbuch, M. Nishioka, A. Ishikawa, and Y. Arakawa, *Observation of the coupled exciton-photon mode splitting in a semiconductor quantum microcavity*, Phys. Rev. Lett. **69**, 3314 (1992).
- [22] I. Carusotto and C. Ciuti, *Quantum fluids of light*, Rev. Mod. Phys. **85**, 299 (2013).
- [23] S. Giorgini, L. P. Pitaevskii, and S. Stringari, *Theory of ultracold atomic Fermi gases*, Rev. Mod. Phys. **80**, 1215 (2008).
- [24] T. Byrnes, T. Horikiri, N. Ishida, and Y. Yamamoto, *BCS Wave-Function Approach to the BEC-BCS Crossover of Exciton-Polariton Condensates*, Phys. Rev. Lett. **105**, 186402 (2010).
- [25] F. Xue, F. Wu, M. Xie, J.-J. Su, and A. H. MacDonald, *Microscopic theory of equilibrium polariton condensates*, Phys. Rev. B **94**, 235302 (2016).
- [26] K. Kamide and T. Ogawa, *What Determines the Wave Function of Electron-Hole Pairs in Polariton Condensates?*, Phys. Rev. Lett. **105**, 056401 (2010).
- [27] K. Kamide and T. Ogawa, *Ground-state properties of microcavity polariton condensates at arbitrary excitation density*, Phys. Rev. B **83**, 165319 (2011).
- [28] J. Levinsen, G. Li, and M. M. Parish, *Microscopic description of exciton-polaritons in microcavities*, Phys. Rev. Research **1**, 033120 (2019).
- [29] See supplemental material for the explicit forms of the variational free energy, further illustrations of the evolution of the state with temperature and density, and discussions of the order of the phase transitions, gauge invariance, behaviour in the limit of no photon coupling,

- the effects of screening and mass imbalance, and numerical methods from Ref. [50].
- [30] G. M. Andolina, F. M. D. Pellegrino, V. Giovannetti, A. H. MacDonald, and M. Polini, *Cavity quantum electrodynamics of strongly correlated electron systems: A no-go theorem for photon condensation*, *Phys. Rev. B* **100**, 121109 (2019).
- [31] K. Rzażewski, K. Wódkiewicz, and W. Żakowicz, *Phase Transitions, Two-Level Atoms, and the A^2 term*, *Phys. Rev. Lett* **35**, 432 (1975).
- [32] P. R. Eastham and P. B. Littlewood, *Bose condensation of cavity polaritons beyond the linear regime: The thermal equilibrium of a model microcavity*, *Phys. Rev. B* **64**, 235101 (2001).
- [33] H. Kleinert, *Path integrals in quantum mechanics, statistics, polymer physics, and financial markets* (World scientific, Singapore, 2009).
- [34] Ref. [10] however neglects intraspecies interactions which may affect its conclusions, see [7].
- [35] A. Tiene, J. Levinsen, M. M. Parish, A. H. MacDonald, J. Keeling, and F. M. Marchetti, *Extremely imbalanced two-dimensional electron-hole-photon systems* (2019), [arXiv:1911.08808](https://arxiv.org/abs/1911.08808).
- [36] J. Keeling, P. R. Eastham, M. H. Szymanska, and P. B. Littlewood, *BCS-BEC crossover in a system of microcavity polaritons*, *Phys. Rev. B* **72**, 115320 (2005).
- [37] D. Bohm, *Note on a Theorem of Bloch Concerning Possible Causes of Superconductivity*, *Phys. Rev.* **75**, 502 (1949).
- [38] We note that in principle a similar statement, that a non-zero photon current and exciton current exist, but cancel at the optimum \mathbf{Q} , also holds for the FF state. However as the FF state is almost entirely dark, this photonic current is negligible.
- [39] T. Brunhes, R. André, A. Arnoult, J. Cibert, and A. Wasiela, *Oscillator strength transfer from X to X^+ in a CdTe quantum-well microcavity*, *Phys. Rev. B* **60**, 11568 (1999).
- [40] R. Rapaport, E. Cohen, A. Ron, E. Linder, and L. N. Pfeiffer, *Negatively charged polaritons in a semiconductor microcavity*, *Phys. Rev. B* **63**, 235310 (2001).
- [41] A. Qarry, R. Rapaport, G. Ramon, E. Cohen, A. Ron, and L. N. Pfeiffer, *Polaritons in microcavities containing a two-dimensional electron gas*, *Semicond. Sci. Technol.* **18**, S331 (2003).
- [42] D. Bajoni, M. Perrin, P. Senellart, A. Lemaître, B. Semage, and J. Bloch, *Dynamics of microcavity polaritons in the presence of an electron gas*, *Phys. Rev. B* **73**, 205344 (2006).
- [43] A. Gabbay, Y. Preezant, E. Cohen, B. M. Ashkinadze, and L. N. Pfeiffer, *Fermi Edge Polaritons in a Microcavity Containing a High Density Two-Dimensional Electron Gas*, *Phys. Rev. Lett.* **99**, 157402 (2007).
- [44] S. Smolka, W. Wuester, F. Haupt, S. Faelt, W. Wegscheider, and A. Imamoglu, *Cavity quantum electrodynamics with many-body states of a two-dimensional electron gas*, *Science* **346**, 332 (2014).
- [45] M. Sidler, P. Back, O. Cotlet, A. Srivastava, T. Fink, M. Kroner, E. Demler, and A. Imamoglu, *Fermi polaron-polaritons in charge-tunable atomically thin semiconductors*, *Nat. Phys.* **13**, 255 (2016).
- [46] B. Chakraborty, J. Gu, Z. Sun, M. Khatoniar, R. Bushati, A. L. Boehmke, R. Koots, and V. M. Menon, *Control of strong light-matter interaction in monolayer WS₂ through electric field gating*, *Nano letters* **18**, 6455 (2018).
- [47] H. A. Fernandez, F. Withers, S. Russo, and W. L. Barnes, *Electrically Tuneable Exciton-Polaritons through Free Electron Doping in Monolayer WS₂ Microcavities*, *Advanced Optical Materials* , 1900484 (2019).
- [48] G. Mahan, *Many-Particle Physics*, Physics of Solids and Liquids (Springer, New York, 2013).
- [49] D. Pimenov, J. von Delft, L. Glazman, and M. Goldstein, *Fermi-edge exciton-polaritons in doped semiconductor microcavities with finite hole mass*, *Phys. Rev. B* **96**, 155310 (2017).
- [50] P. Virtanen, R. Gommers, T. E. Oliphant, M. Haberland, T. Reddy, D. Cournapeau, E. Burovski, P. Peterson, W. Weckesser, J. Bright, S. J. van der Walt, M. Brett, J. Wilson, K. Jarrod Millman, N. Mayorov, A. R. J. Nelson, E. Jones, R. Kern, E. Larson, C. Carey, Í. Polat, Y. Feng, E. W. Moore, J. VanderPlas, D. Laxalde, J. Perktold, R. Cimrman, I. Henriksen, E. A. Quintero, C. R. Harris, A. M. Archibald, A. H. Ribeiro, F. Pedregosa, P. van Mulbregt, and SciPy 1.0 Contributors, *SciPy 1.0—Fundamental Algorithms for Scientific Computing in Python*, (2019), [1907.10121](https://doi.org/10.10121).

SUPPLEMENTARY MATERIAL FOR: “CRESCENT STATES IN CHARGE-IMBALANCED POLARITON CONDENSATES”

VARIATIONAL FREE ENERGY

We provide here explicit expressions for the variational free energy, F_v . To derive this, we note that diagonalising the Hamiltonian in Eq. (4) requires a shift of the photon operator, $\hat{a}_{\mathbf{Q}} \rightarrow \hat{a}_{\mathbf{Q}} - \sqrt{S}\phi$. The fermionic part of the Hamiltonian is diagonalised by a unitary transform:

$$\begin{pmatrix} \hat{c}_{\mathbf{Q}/2+\mathbf{k}} \\ \hat{h}_{\mathbf{Q}/2-\mathbf{k}}^\dagger \end{pmatrix} = \begin{pmatrix} u_{\mathbf{k}} & v_{\mathbf{k}} \\ -v_{\mathbf{k}} & u_{\mathbf{k}} \end{pmatrix} \begin{pmatrix} \hat{c}_{+,\mathbf{k}} \\ \hat{c}_{-,\mathbf{k}}^\dagger \end{pmatrix}, \quad (\text{S1})$$

where

$$u_{\mathbf{k}} = \sqrt{\frac{1}{2} \left(1 + \frac{\eta_{\mathbf{k}}^e + \eta_{\mathbf{k}}^h}{2E_{\mathbf{k}}} \right)}, \quad (\text{S2a})$$

$$v_{\mathbf{k}} = -\text{sign}(\Delta_{\mathbf{k}}) \sqrt{\frac{1}{2} \left(1 - \frac{\eta_{\mathbf{k}}^e + \eta_{\mathbf{k}}^h}{2E_{\mathbf{k}}} \right)}, \quad (\text{S2b})$$

$$E_{\mathbf{k}} = \sqrt{\left(\frac{\eta_{\mathbf{k}}^e + \eta_{\mathbf{k}}^h}{2} \right)^2 + \Delta_{\mathbf{k}}^2}. \quad (\text{S2c})$$

We define the resulting eigenvalues of the diagonalised Fermionic problem as

$$\varepsilon_{\mathbf{k}}^\pm = E_{\mathbf{k}} \pm (\eta_{\mathbf{k}}^e - \eta_{\mathbf{k}}^h)/2. \quad (\text{S3})$$

Using this, expressions such as the electron $N_{\mathbf{k}}^e = \langle \hat{c}_{\mathbf{k}+\mathbf{Q}/2}^\dagger \hat{c}_{\mathbf{k}+\mathbf{Q}/2} \rangle$ and hole $N_{\mathbf{k}}^h = \langle \hat{h}_{\mathbf{Q}/2-\mathbf{k}}^\dagger \hat{h}_{\mathbf{Q}/2-\mathbf{k}} \rangle$ populations can be expressed in terms of variational parameters via:

$$N_{\mathbf{k}}^e = u_{\mathbf{k}}^2 n_F(\varepsilon_{\mathbf{k}}^+) + v_{\mathbf{k}}^2 [1 - n_F(\varepsilon_{\mathbf{k}}^-)],$$

$$N_{\mathbf{k}}^h = v_{\mathbf{k}}^2 [1 - n_F(\varepsilon_{\mathbf{k}}^+)] + u_{\mathbf{k}}^2 n_F(\varepsilon_{\mathbf{k}}^-),$$

where $n_F(\varepsilon)$ is the Fermi distribution. Because the variational state is Gaussian, the expectations of quartic terms in the Hamiltonian can be decoupled via Wick's theorem. When putting this all together, we will first take the continuum (large S limit), where momentum sums become integrals. Then, as described in the main text, we use $a_B = \varepsilon/(2\mu e^2)$ as a lengthscale, and so introduce a dimensionless momentum $\tilde{\mathbf{k}} = a_B \mathbf{k}$. We thus find:

$$\begin{aligned} \frac{F_v}{S a_B^{-2}} = & - \int \frac{d\tilde{\mathbf{k}}}{(2\pi)^2} \left[\varepsilon_{\mathbf{k}}^+ n_F(\varepsilon_{\mathbf{k}}^+) + \frac{1}{\beta} \ln \left(1 + e^{-\beta \varepsilon_{\mathbf{k}}^+} \right) + (\varepsilon_{\mathbf{k}}^+ \rightarrow \varepsilon_{\mathbf{k}}^-) \right] + \frac{\alpha}{a_B^2} \left\{ \iint \frac{d\tilde{\mathbf{k}} d\tilde{\mathbf{k}}'}{(2\pi)^4} N_{\mathbf{k}}^c N_{\mathbf{k}'}^c - 2n_0 a_B^2 \int \frac{d\tilde{\mathbf{k}}}{(2\pi)^2} N_{\mathbf{k}}^c \right\} \\ & + \frac{E_{ee}^X + E_{hh}^X}{S a_B^{-2}} - \iint \frac{d\tilde{\mathbf{k}} d\tilde{\mathbf{k}}'}{(2\pi)^4} \left\{ \frac{V_{\mathbf{k}-\mathbf{k}'}}{a_B^2} u_{\mathbf{k}} v_{\mathbf{k}} \left[1 - n_F(\varepsilon_{\mathbf{k}}^+) - n_F(\varepsilon_{\mathbf{k}'}^+) \right] u_{\mathbf{k}'} v_{\mathbf{k}'} \left[1 - n_F(\varepsilon_{\mathbf{k}'}^+) - n_F(\varepsilon_{\mathbf{k}}^-) \right] \right\} \\ & + \int \frac{d\tilde{\mathbf{k}}}{(2\pi)^2} \left\{ E_{\mathbf{k}+\frac{\mathbf{Q}}{2}}^e N_{\mathbf{k}}^e + E_{\frac{\mathbf{Q}}{2}-\mathbf{k}}^h N_{\mathbf{k}}^h \right\} + \phi^2 a_B^2 (\omega_{\mathbf{Q}} - \mu_{ex}) + 2\phi a_B \int \frac{d\tilde{\mathbf{k}}}{(2\pi)^2} \frac{g_{\mathbf{k}+\frac{\mathbf{Q}}{2}}}{a_B} u_{\mathbf{k}} v_{\mathbf{k}} \left[n_F(\varepsilon_{\mathbf{k}}^+) + n_F(\varepsilon_{\mathbf{k}}^-) - 1 \right]. \quad (\text{S4}) \end{aligned}$$

Here $N_{\mathbf{k}}^c = N_{\mathbf{k}}^e - N_{\mathbf{k}}^h$, the bare electronic energies are:

$$E_{\mathbf{k}}^e = E_B \frac{m_h \tilde{k}^2}{m_e + m_h} + E_G - \frac{1}{2} \mu_{ex}, \quad (\text{S5a})$$

$$E_{\mathbf{k}}^h = E_B \frac{m_e \tilde{k}^2}{m_e + m_h} - \frac{1}{2} \mu_{ex}, \quad (\text{S5b})$$

written in terms of $E_B = 1/(2\mu a_B^2)$ and the exchange energies

$$\frac{E_{ee}^X}{S a_B^{-2}} = -\frac{1}{2} \iint \frac{d\tilde{\mathbf{k}} d\tilde{\mathbf{k}}'}{(2\pi)^4} N_{\mathbf{k}}^{e/h} \frac{V_{\mathbf{k}-\mathbf{k}'}}{a_B^2} N_{\mathbf{k}'}^{e/h}. \quad (\text{S6})$$

We may note that in Eq. (S4), the quantities $n_0 a_B^2$ and ϕa_B are dimensionless, while α/a_B^2 , $V_{\mathbf{p}}/a_B^2$ and $g_{\mathbf{p}}/a_B$ have units of energy as expected. For the Coulomb in-

teractions, we may define:

$$v_{\tilde{\mathbf{p}}} \equiv \frac{V_{\tilde{\mathbf{p}}}}{a_B^2} = \frac{2\pi E_B}{\tilde{p}} \quad (\text{S7})$$

Since we include the global electrostatic energy explicitly, we use a definition where V_0 is set to zero.

Numerical evaluation

At each point in the numerical minimisation, one must evaluate the energy and its derivatives. Calculation of the expectation of the Coulomb interactions requires a 4D integral of the form

$$I_C = \iint d\tilde{\mathbf{k}} d\tilde{\mathbf{k}}' f(\tilde{\mathbf{k}}) v_{\tilde{\mathbf{k}}-\tilde{\mathbf{k}}'} f(\tilde{\mathbf{k}}').$$

Evaluating this on a grid of $N \times N$ points would require N^4 operations, significantly limiting the values of N that can be used. However, by rewriting this integral one can significantly reduce the computational effort involved. Using the Fourier transform $\tilde{f}(\tilde{\mathbf{x}}) \equiv \int d\tilde{\mathbf{k}} f(\tilde{\mathbf{k}}) e^{i\tilde{\mathbf{k}} \cdot \tilde{\mathbf{x}}} / (2\pi)^2$, one can rewrite I_C as a 2D integral in real space $I_C = \int d\tilde{\mathbf{x}} |\tilde{f}(\tilde{\mathbf{x}})|^2 \tilde{v}(\tilde{\mathbf{x}})$, which now requires only N^2 operations. At the same time, Fast Fourier Transform of a 2D function requires $O(N^2 \ln N)$ operations. Therefore, calculating the integral I_C in real space reduces the scaling of the number of operations from N^4 to $N^2 \ln N$ allowing to do the full 2D optimisation efficiently on a reasonable momentum grid, e.g. for 10^4 k -points. To implement the above idea, in the second line of Eq. (S4) we define $f(\tilde{\mathbf{k}}) = u_{\mathbf{k}} v_{\mathbf{k}} [1 - n_F(\varepsilon_{\mathbf{k}}^+) - n_F(\varepsilon_{\mathbf{k}}^-)]$. Exchange energies can be rewritten in the same way: $E_{ee/hh}^X = -\frac{1}{2} \int d\mathbf{x} |\tilde{N}^{e/h}(\mathbf{x})|^2 \tilde{v}(\mathbf{x})$.

We numerically implement the minimisation by using the truncated Newton algorithm from the SciPy [50] library. As local minima can exist in the free energy landscape (see below), we use a method equivalent to an adiabatic sweep. Specifically, as we vary a control parameter, we use the optimal variational parameters found for one value of the control parameter as initial conditions for the minimisation at the next value of the control parameter. As discussed further below, where there can be hysteresis, we use repeated sweeps with increasing and decreasing control parameters.

ELECTRON, HOLE AND COHERENCE CROSS SECTIONS AT $k_y = 0$

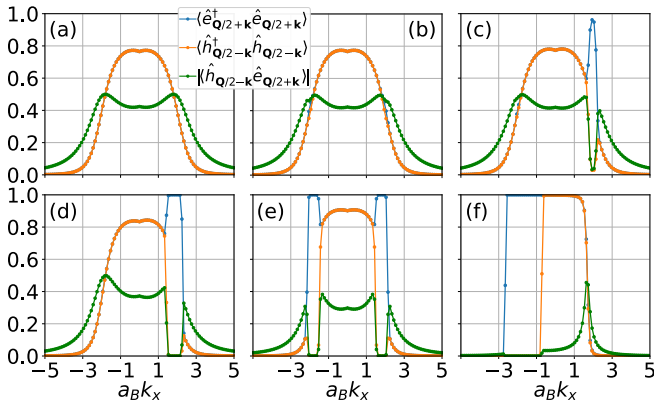


Figure S1. Cross sections at $k_y = 0$, showing the electron and hole populations, and electron-hole coherence. Panels shown here correspond to those shown in Fig. 2 of the main text.

Figures S1 and S2 show cross sections of the electron and hole densities and the coherence function at varying charge density and temperature. In plotting these figures, the rotational symmetry breaking is always chosen such that there is symmetry about the $k_y = 0$ line, so

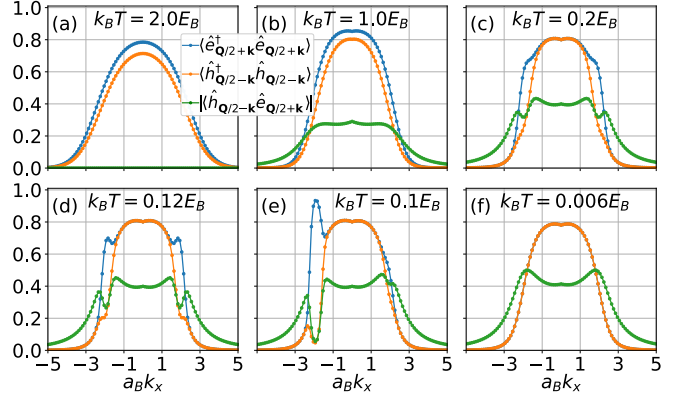


Figure S2. Cross sections at $k_y = 0$ for various temperatures as indicated, for charge density $n_0 a_B^2 = 0.075$. All other parameters as in Fig. 1 of the main text.

that any crescent will intersect the cross section shown. As also discussed in the caption of Fig. 1 of the main text, these cross sections show that within the crescent or ring, both conduction and valence bands are occupied, while at other momenta, a total of one band is filled, so that electron and hole populations are equal. At low enough temperatures, the crescent or breached pair states show a complete suppression of the hole population within the Fermi surface. When the temperature becomes comparable to the conduction band Fermi energy, the suppression is weaker.

FIRST-ORDER PHASE TRANSITIONS

As seen from the evolution of the anisotropy order parameter with charge imbalance shown in Fig. 3, the transition from the crescent state (CS) to the breached pair (BP) state is discontinuous. This indicates the transition is first order, associated with the existence of two distinct local minima of the free energy. Figure S3 shows that corresponding to this, one sees hysteresis in the anisotropy, as measured by comparing an adiabatic sweep of increasing vs decreasing the charge density n_0 .

As well as the existence of separate local minima for the CS and BP state, one can also find parameter regimes where the CS and FF state solutions exist as competing local minima. Indeed, as seen from the phase diagram, Fig. 4, at large photon energy ω_0 , there is a direct CS-FF transition. Figure S4 illustrates this, showing the free energy landscape vs Q and the solutions corresponding to the two local minima.

GAUGE INVARIANCE

As mentioned in the Letter, the exponential momentum cutoff κ for the matter-light interaction regularise

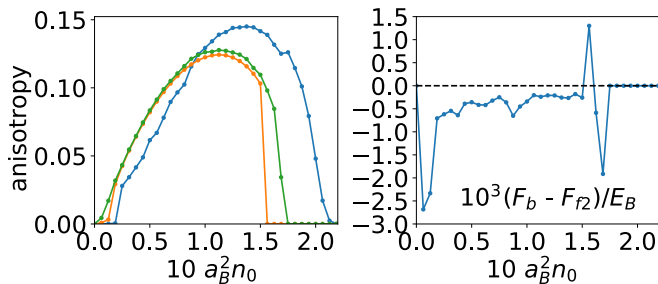


Figure S3. Hysteresis associated with the counterflow condensate to breached pair transition. Data is collected using adiabatic sweeps of charge density (i.e. using minimum found at the previous value of n_0 as the initial guess for the next value of n_0). Three sweeps are shown; first increasing n_0 (f1), then decreasing n_0 (b) and then again increasing n_0 (f2). The first forward sweep did not achieve a global minimum so should be discarded; the subsequent sweeps do find consistent solutions for most n_0 , but hysteresis is seen around the CS-BP transition. All other parameters are as in Fig. 1.

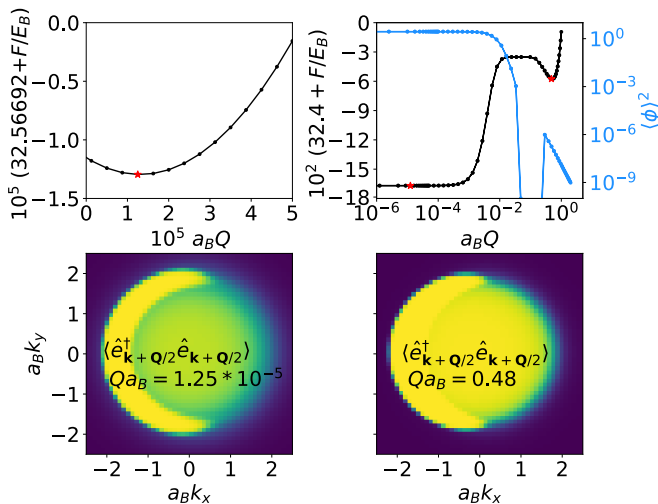


Figure S4. Coexisting local minima corresponding to counterflow condensate and FFLO states. Top panels show the free energy and photon order parameter vs pairing wavevector Q . The top left panel is an expanded region of small Q around the optimal wavevector for the CS state. The bottom two panels show the electron mode occupation for the CS (left) and FF (right) solutions, corresponding to the red stars shown in the top panels. Parameters are $n_0 a_B^2 = 0.1$, $\omega_0 = 3.1 E_B$, and all other parameters as in Fig. 1

the UV divergence, but breaks gauge invariance. In this section we discuss the consequence of this and a possible way to restore the gauge invariance by considering $\kappa \rightarrow \infty$ and renormalising the photon frequency [28]. We focus here on the invariance under transformations involving a static and uniform change of the vector potential, as these are sufficient to understand the issues introduced by the cutoff κ . A more complete discussion of the necessity of gauge invariant models when considering ground-state phase transitions can be found in Ref. [30].

Consider a simple gauge transformation by adding a constant vector-potential to the electron and hole momenta, $\mathbf{k} \rightarrow \mathbf{k} \pm e\mathbf{A}$, where e is the electronic charge, and the sign of shift depends on the type of quasiparticle. After this shift the kinetic energy part of the Hamiltonian then becomes:

$$\sum_{\mathbf{k}} \frac{1}{2m} \left\{ (\mathbf{k} + e\mathbf{A})^2 \hat{e}_{\mathbf{k}}^\dagger \hat{e}_{\mathbf{k}} + (\mathbf{k} - e\mathbf{A})^2 \hat{h}_{\mathbf{k}}^\dagger \hat{h}_{\mathbf{k}} \right\}. \quad (\text{S8})$$

To be gauge invariant, the model must be invariant under this transformation. Relabeling operators $\hat{e}_{\mathbf{k}} \rightarrow \hat{e}_{\mathbf{k}+e\mathbf{A}}$ and $\hat{h}_{\mathbf{k}} \rightarrow \hat{h}_{\mathbf{k}-e\mathbf{A}}$ clearly recovers the original kinetic part of the Hamiltonian. One can also readily check that this relabeling does not affect the Coulomb term. However, it does change the matter-light interaction term $\sum_{\mathbf{k}} g_{\mathbf{k}} \hat{e}_{\mathbf{k}}^\dagger \hat{h}_{\mathbf{q}-\mathbf{k}}^\dagger \hat{a}_{\mathbf{q}}$, as this now becomes:

$$\sum_{\mathbf{k}} g_{\mathbf{k}} \hat{e}_{\mathbf{k}+e\mathbf{A}}^\dagger \hat{h}_{\mathbf{q}-\mathbf{k}-e\mathbf{A}}^\dagger \hat{a}_{\mathbf{q}} = \sum_{\mathbf{k}} g_{\mathbf{k}-e\mathbf{A}} \hat{e}_{\mathbf{k}}^\dagger \hat{h}_{\mathbf{q}-\mathbf{k}}^\dagger \hat{a}_{\mathbf{q}}. \quad (\text{S9})$$

One clearly sees that the momentum dependence of the coupling constant makes the model gauge dependent.

The total charge current can be related to the derivative of the free energy with respect to vector potential, i.e. $\mathbf{j}_{\mathbf{A}} = dF/d\mathbf{A}$. Since the free energy F of a gauge-invariant model cannot depend on a constant gauge shift, the charge current in such a case is identically zero. However, since our model breaks the gauge invariance, $F(\mathbf{A})$ has a minimum at a non-zero value of \mathbf{A} , which implies a finite charge current at $\mathbf{A} = \mathbf{0}$, $\mathbf{j}_0 = dF/d\mathbf{A}|_{\mathbf{A}=\mathbf{0}}$.

To recover gauge invariance within our model, one needs a momentum independent coupling $g_{\mathbf{k}}$, or equivalently, to send the cut-off to infinity, $\kappa \rightarrow \infty$. This introduces an ultraviolet divergence, however, as shown in Ref. [28], this divergence can be removed renormalising the bare photon frequency. Following Ref. [28], one can show that to keep the renormalised photon frequency constant under a change in the momentum cutoff from κ_1 to κ_2 requires a shift of the bare photon energy ω_0 . At large κ this shift is approximately given by $\delta\omega_0 \approx (g_0^2 \mu / \pi) \ln(\kappa_2 / \kappa_1)$. In Fig. S5 we plot $F(\mathbf{A})$ for various values of the cutoff, $\kappa a_B = 2.5, 3.75, 5.0$. In plotting this figure, we in fact choose the value ω_0 at each cutoff κ so as to ensure that the free energy at $A = 0$ remains constant. Note that this means that in this figure we implicitly use a renormalisation scheme where the shift of ω_0 is chosen for the non-zero value of n_0 used in this figure. The bare frequencies used are given in the caption.

From Fig. S5 we see firstly that the overall scale of the current (or equivalently the variation of the $F(\mathbf{A})$ with \mathbf{A}) reduces with increasing cutoff. Moreover, in the right panels of this figure we plot the electron mode occupations at the minimum of $F(\mathbf{A})$, A_{min} , for $\kappa a_B = 2.5, 5.0$. It is clear that changing the cutoff does not significantly change the electron distribution. These results suggest

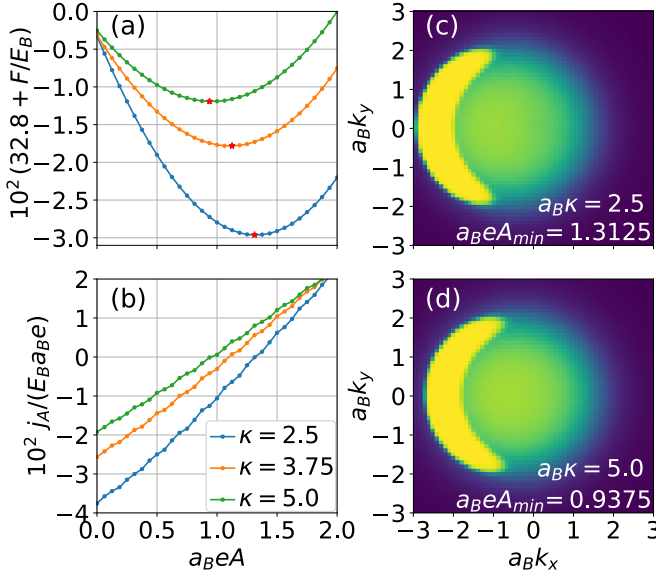


Figure S5. (a) Free energy $F(\mathbf{A})$ versus constant vector potential shift \mathbf{A} and (b) corresponding charge current, $\mathbf{j}_A = dF(\mathbf{A})/d\mathbf{A}$. The three lines correspond to photon cutoff frequency and momentum cutoffs $\omega_0 = 3.06E_B$, $\kappa = 2.5a_B^{-1}$ (blue), $\omega_0 = 3.1055E_B$, $\kappa = 3.75a_B^{-1}$ (orange) and $\omega_0 = 3.1435E_B$, $\kappa = 5.0a_B^{-1}$ (green). (c,d) electron occupations at the positions of the free energy minima for $\kappa = 2.5a_B^{-1}$ and $\kappa = 5.0a_B^{-1}$. Target charge density $n_0 a_B^2 = 0.1$; all other parameters are the same as in the main part of the paper.

that, in the limit $\kappa \rightarrow \infty$, by renormalising the bare photon frequency, we obtain gauge invariant results, which remain qualitatively the same as those we found with a finite cutoff.

SECOND-ORDER BC-FF PHASE TRANSITION WITHOUT A PHOTON, $m_e = m_h$

In this section we present the behaviour of the purely excitonic system, using the explicit gating scheme we consider to fix the charge density. Previous work [10] found a first order transition between a balanced condensate phase and an FFLO state, by working in the grand canonical ensemble and thus introducing a chemical potential for imbalance, $H \rightarrow H - \mu_c S n_c$. However, Ref. [10] also neglected intraspecies interactions, i.e. electron-electron and hole-hole repulsion. Subasi *et al.* [7] in contrast found that including such intraspecies interactions makes phase transitions continuous. Here, we show that with our explicit gating process and including intraspecies interactions, even in the absence of photons, we indeed observe a second order transition, with the pairing Q -vector growing continuously as density imbalance increases — see Fig. S6. As shown in the figure, we in fact find that, within our gating model, a narrow region of a weakly breached pair state exists between the balanced conden-

sate and FFLO states — i.e. a state with excess charge density on a ring near the Fermi surface.

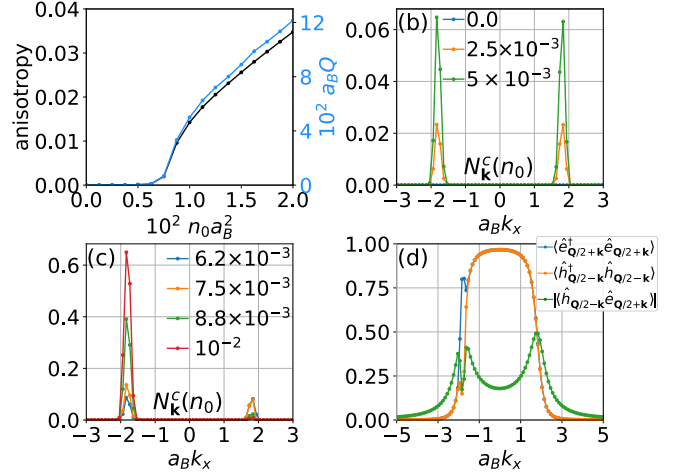


Figure S6. Second order phase transitions for the excitonic limit (no coupling to light). (a) Evolution of anisotropy (black, left) and center of mass momentum Q (blue, right) vs increasing density imbalance n_0 . (b) Momentum resolved net charge distribution $N_{\mathbf{k}}^c = \langle \hat{e}_{\mathbf{Q}/2+\mathbf{k}}^\dagger \hat{e}_{\mathbf{Q}/2+\mathbf{k}} - \hat{h}_{\mathbf{Q}/2-\mathbf{k}}^\dagger \hat{h}_{\mathbf{Q}/2-\mathbf{k}} \rangle$ at small imbalance, showing a weakly BP state. (c) Same quantity at larger imbalance, showing the appearance of the FF state. (d) Electron and hole occupation, coherence at $n_0 a_B^2 = 0.01$ — just into the FF state. Note the opposite momentum offset for electron and hole states.

ENERGETIC ORIGIN OF THE CS STATE

Effects of screening on the CS state

While it is the coupling to light which stabilizes $\mathbf{Q} \simeq \mathbf{0}$ imbalanced states vs FF states, in this section we prove that the anisotropic crescent state also requires long-ranged Coulomb interactions. To demonstrate this, Fig. S7 shows how the anisotropy changes as we introduce screening of the Coulomb interaction. We consider a Yukawa potential, $V_{\mathbf{k}}(\kappa_S) = 2\pi e^2 / \varepsilon(k + \kappa_S)$, where $1/\kappa_S$ is a screening length, such that $\kappa_S = 0$ recovers the unscreened Coulomb interaction. As seen in Fig. S7, the anisotropy vanishes when the screening length approaches the bare exciton Bohr radius. From the colormaps, we see that as anisotropy vanishes, the crescent state is replaced by the breached pair state.

Competition of kinetic and Coulomb energies

Figure S8 provides further evidence that the Coulomb interactions are important in driving the formation of the anisotropic phase. In this figure we show the electronic kinetic and Coulomb energies vary as we cross the

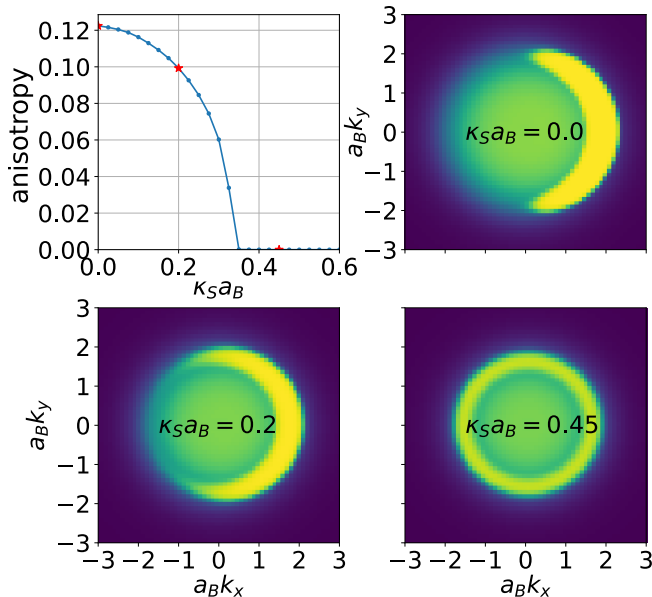


Figure S7. Effect of screening $V_{\mathbf{k}}(\kappa_S) = 2\pi e^2/\varepsilon(k + \kappa_S)$; $n_0 a_B^2 = 0.1$, $\omega_0 = 3.06 E_B$, other parameters are the same as in Fig. 1. Top left panel shows the dependence of anisotropy on screening. Other panels show electron occupations corresponding to points highlighted by red crosses.

boundary between the CS and BP phase. For the first order transition with increasing target charge density, we see clearly that the first order boundary is a competition between the CS state, with higher kinetic energy and lower exchange, and the BP state with lower kinetic energy but higher exchange. This confirms the conclusion above that it is the long-range Coulomb interaction which favours the CS state.

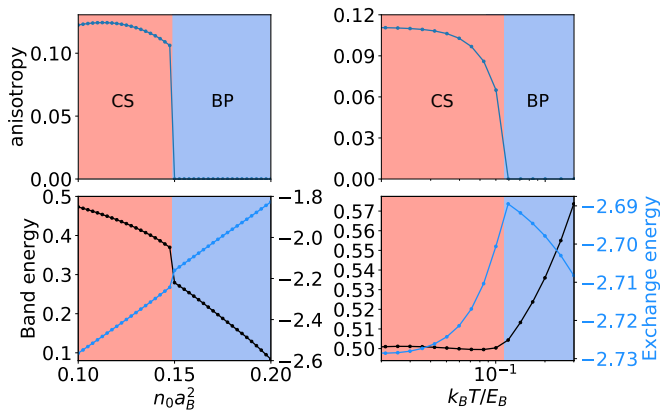


Figure S8. Energy decomposition of free energy at the boundary of CS and BP phases. Top left and right panels show, for reference, anisotropy versus charge density $n_0 a_B^2$ and temperature T respectively. Bottom panels show corresponding kinetic energy (sum of electron and hole kinetic energies) and exchange energy (total of electron-electron, hole-hole and electron-hole terms). All parameters are the same as in left and right panels of Fig. 3 respectively.

MASS IMBALANCE

In the Letter, we presented results only for the case where the conduction and valence band have equal masses. In this section, we show how mass imbalance — which is usually present in real materials — affects the CS state.

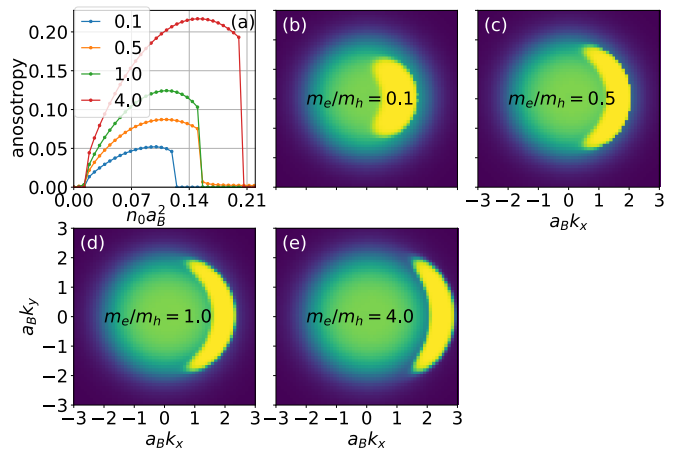


Figure S9. (a) Anisotropy versus target charge density n_0 at different mass imbalance. (b-e) electron occupations at $n_0 a_B^2 = 0.075$ corresponding to different mass ratios as labelled. All other parameters are the same as in Fig. 1.

In Fig. S9 we plot the dependence of anisotropy on n_0 , and the electron occupations at $n_0 = 0.075 a_B^{-2}$, for four values of m_e/m_h ranging from 0.1 to 4.0. Typically electron mass is lower than the hole mass, $m_e/m_h < 1$. However, since our Hamiltonian is invariant under a transformation $e \leftrightarrow h, n_0 \rightarrow -n_0$, one can consider the behaviour for $m_e/m_h > 1$ as indicating the behaviour when there is hole doping rather than electron doping.

Clearly, all results are qualitatively the same, although as seen from Fig. S9(a), a reduced mass ratio shrinks the range of n_0 where the CS state occurs. In addition, changing mass ratio distorts the region of momentum space where the extra electrons are found. Heavier electrons — Fig. S9(e) — lead to a more extended crescent, while lighter electrons to a less extended one — Fig. S9(b).

At yet higher target charge densities n_0 , the system adopts either the FF state or a normal state. When the mass ratio m_e/m_h becomes small (for electron doping), the FF state becomes less stable, and is replaced by the normal state [10]. This comes from the increased separation of electron and hole Fermi surfaces when $m_e \ll m_h$ and $n_e > n_h$. In contrast, the opposite mass ratio brings Fermi energies closer.